the FEBS Journal

Kinetic and crystallographic analyses of the catalytic domain of chitinase from *Pyrococcus furiosus* – the role of conserved residues in the active site

Hiroaki Tsuji[1], Shigenori Nishimura[1], Takashi Inui[1], Yuji Kado[2], Kazuhiko Ishikawa[2], Tsutomu Nakamura[2] and Koichi Uegaki[2]

1 Laboratory of Protein Sciences, Graduate School of Life and Environmental Sciences, Osaka Prefecture University, Japan
2 National Institute of Advanced Industrial Science and Technology, Osaka, Japan

Keywords
chitinase; crystal structure; DXDXE motif; glycoside hydrolase family; *Pyrococcus furiosus*

Correspondence
S. Nishimura, Laboratory of Protein Sciences, Graduate School of Life and Environmental Sciences, Osaka Prefecture University, 1-1 Gakuencho, Sakai, Osaka 599-8531, Japan
Fax: +81 72 254 9462
Tel: +81 72 254 9462
E-mail: tigers@bioinfo.osakafu-u.ac.jp
K. Uegaki, National Institute of Advanced Industrial Science and Technology, 1-8-31 Midorigaoka, Ikeda, Osaka 563-8577, Japan
Fax: +81 72 751 8370
Tel: +81 72 751 9526
E-mail: k-uegaki@aist.go.jp

Database
Structural data are available at the Protein Data Bank under the accession numbers 3A4W (E526A–substrate complex), 3A4X (D524A–substrate complex) and 3AFB (D524A apo-form)

(Received 25 February 2010, revised 10 April 2010, accepted 13 April 2010)

doi:10.1111/j.1742-4658.2010.07685.x

The hyperthermostable chitinase from the hyperthermophilic archaeon *Pyrococcus furiosus* has a unique multidomain structure containing two chitin-binding domains and two catalytic domains, and exhibits strong crystalline chitin hydrolyzing activity at high temperature. In order to investigate the structure–function relationship of this chitinase, we analyzed one of the catalytic domains (AD2) using mutational and kinetic approaches, and determined the crystal structure of AD2 complexed with chito-oligosaccharide substrate. Kinetic studies showed that, among the acidic residues in the signature sequence of family 18 chitinases (DXDXE motif), the second Asp (D_2) and Glu (E) residues play critical roles in the catalysis of archaeal chitinase. Crystallographic analyses showed that the side-chain of the catalytic proton-donating E residue is restrained into the favorable conformer for proton donation by a hydrogen bond interaction with the adjacent D_2 residue. The comparison of active site conformations of family 18 chitinases provides a new criterion for the subclassification of family 18 chitinase based on the conformational change of the D_2 residue.

Introduction

Chitin, a highly stable homopolysaccharide of β-(1,4)-linked *N*-acetyl-D-glucosamine (NAG), is an important structural component of the shells of insects and crustaceans, fungal cell walls and the exoskeletons of

Abbreviations
AD, active (catalytic) domain; BcChiA1, chitinase A1 from *Bacillus circulans*; CcCTS1, chitinase 1 from *Coccidioides immitis*; ChBD, chitin-binding domain; GH, glycoside hydrolase; NAG, *N*-acetyl-β-D-glucosamine; $(NAG)_n$, β-(1,4)-linked oligomers of NAG residue where n = 1–6; Pf-ChiA, chitinase from *Pyrococcus furiosus*; PNP-$(NAG)_2$, *p*-nitrophenyl-chitobiose; ScCTS1, chitinase 1 from *Saccharomyces cerevisiae*; SmChiB, chitinase B from *Serratia marcescens*; TK-ChiA, chitinases A from *Thermococcus kodakaraensis*.

arthropods. Chitinases (EC 3.2.1.14) are important enzymes that hydrolyze chitin into smaller chito-oligosaccharide fragments. They are found in a wide range of organisms, including bacteria, fungi, plants and animals. The presence of chitinases in such organisms is closely associated with the physiological roles of their substrates. For instance, bacteria produce chitinases so that they can use chitin as a source of carbon and nitrogen for growth [1–3], whereas chitinases in yeasts and other fungi are important for autolysis, nutritional and morphogenetic functions [4,5]. Plant chitinases play a role as defensive agents against pathogenic fungi and some parasites by disrupting their cell walls [6–8], whereas viral chitinases are involved in the pathogenesis of host cells. Animal chitinases are involved in dietary uptake processes [9]. Human chitinases are particularly associated with anti-inflammatory effects against T-helper-2-driven diseases, such as allergic asthma [10–12].

In a classification of glycoside hydrolases (GHs) based on amino acid sequence similarity, established by Henrissat and coworkers [13–15], chitinases are classified into two different families: GH families 18 and 19 [described in the carbohydrate active enzyme (CAZy) database, http://www.cazy.org/]. These two families show no homology in either primary or tertiary structures. Family 19 chitinases are almost exclusively derived from plants, and have a high degree of sequence similarity. The catalytic domain of family 19 chitinases comprises two lobes, each of which is rich in α-helical structure [16,17]. In contrast, family 18 includes chitinases from microbes, plants and animals, and has a substantial sequence divergence. In spite of their diverse primary structures, all the catalytic domains of family 18 chitinases have a common TIM-barrel $(\beta/\alpha)_8$-fold [18–23] and are characterized by a highly conserved signature sequence (DXDXE motif) on the β4-strand (Fig. 1). The Glu (E) in this motif acts as the catalytic proton donor, and the second Asp (D_2) is supposed to contribute to the stabilization of the essential distortion of the substrate [24].

We have reported previously that PF1234 and PF1233, which are adjacent open reading frames of the hyperthermophilic archaeon *Pyrococcus furiosus* with an interval of 37 bp [25], are homologous to the first and second halves, respectively, of a chitinase from *Thermococcus kodakaraensis* (TK-ChiA) [26]. We

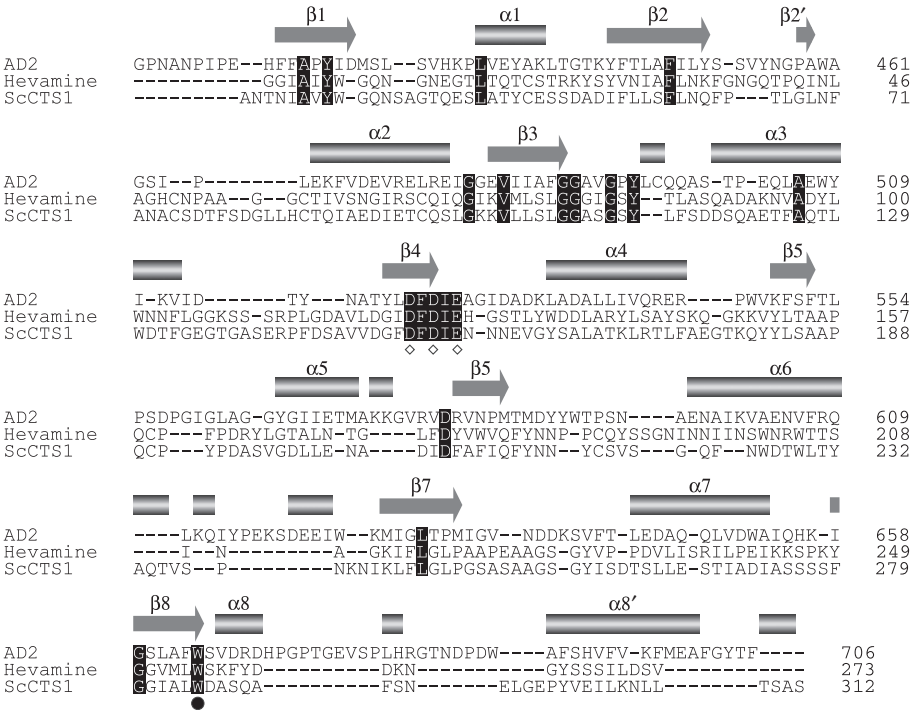

Fig. 1. Sequence alignment of three family 18 chitinases based on secondary structure similarity. AD2, hevamine from *Hevea brasiliensis* and chitinase 1 from *Saccharomyces cerevisiae* (ScCTS1) are shown. The overall conserved amino acid residues are highlighted in black boxes. Conserved secondary structure elements are indicated above the sequence alignment. The open diamonds represent the highly conserved (among family 18 chitinases) DXDXE motif, and the filled circle represents the solvent-exposed tryptophan residue. The alignment was performed using the MATRAS server (http://biunit.naist.jp/matras/).

combined them into one gene by a frame shift mutation, and the gene product yielded a recombinant chitinase (Pf-ChiA) homologous to TK-ChiA. Interestingly, Pf-ChiA effectively hydrolyzed not only colloidal chitin, but also crystalline chitin [25]. The optimum temperature of Pf-ChiA for the hydrolysis of crystalline chitin was extremely high, measured to be over 90 °C. Recently, the enzymatic degradation of chitin waste using chitinases has attracted much attention as an environmentally friendly alternative to conventional chemical degradation methods, because chitin derivatives provide a diverse range of applications in areas such as biomedicines, food additives and cosmetics [27]. Hence Pf-ChiA, which exhibits hyperthermostability and high hydrolyzing activity towards crystalline chitin, is useful as an efficient catalyst for the bioconversion of chitin into valuable oligosaccharide derivatives for various industrial applications.

Pf-ChiA has a unique multidomain structure containing two chitin-binding domains (ChBD1 and ChBD2) and two catalytic (active) domains (AD1 and AD2) [25]. Both catalytic domains belong to GH family 18. We have not performed any kinetic or structural studies of the complete Pf-ChiA because of its low expression level in *Escherichia coli*, but have focused instead on the properties of the individual domains. We have already determined the structures of ChBD2 and AD2 by means of NMR spectroscopy and X-ray crystallography, respectively [23,28]. We found that the overall structure of AD2 is a TIM-barrel $(\beta/\alpha)_8$-fold with a groove-like active site architecture, which is a typical feature of endo-chitinases.

As with other family 18 chitinases, AD2 contains a highly conserved DXDXE motif [corresponding to Asp522(D_1)-Ile523-Asp524(D_2)-Phe525-Glu526(E)] on the β4-strand (Fig. 1). In this study, we focused on these three conserved acidic residues in AD2 and carried out mutational and crystallographic analyses in order to clarify their catalytic role. Our kinetic study indicated that D_2 and E residues play particularly important roles in catalysis. By using AD2 D524A and E526A mutants, whose enzymatic activities have been greatly depressed, we determined the crystal structures of these mutants complexed with chito-oligosaccharide substrate. The results of the kinetic analyses confirmed that the Glu526 residue has a proton-donating function like other family 18 chitinases. Asp524 was considered to act to restrain the side-chain of catalytic Glu526 into the favorable conformer for proton donation by hydrogen bond interaction. In addition, by comparing the structures of AD2 with those of other family 18 chitinases, we proposed a new criterion for the subclassification of family 18 chitinases with respect to the conformational change of the D_2 residue on substrate binding, as well as the overall folding.

Results

Site-directed mutagenesis and enzyme purification

First, we constructed a number of single point mutants of AD2 by site-directed mutagenesis. Figure 1 shows the sequence alignment of three family 18 chitinases. The side-chains of three residues (Asp522, Asp524 and Glu526) in the DXDXE motif were mutated into the corresponding amide (Asn or Gln) and Ala. All the AD2 mutants (D522N, D522A, D524N, D524A, E526Q and E526A) were overexpressed in *E. coli* and purified by the same procedures as the wild-type enzyme described previously [29]. Far-UV CD spectra (200–255 nm) of AD2 wild-type and all mutants at 25, 50 and 85 °C were almost identical (data not shown), indicating that all the mutant enzymes retained thermostability and similar secondary structures.

Kinetic properties of AD2 mutants

Table 1 shows the apparent kinetic constants k_{cat} and K_m for the hydrolysis of *p*-nitrophenyl-chitobiose [PNP-$(NAG)_2$] catalyzed by seven enzymes (wild-type, D522N, D522A, D524N, D524A, E526Q and E526A). The D522N and D522A mutants retained about 40% and 20%, respectively, of the wild-type k_{cat} values. The D524N mutation increased the K_m value slightly, and decreased the k_{cat} value by about 2.7-fold. These k_{cat} and K_m values were comparable with those of Asp522 mutants (D522N and D522A). In contrast, the D524A mutation affected both k_{cat} and K_m values significantly, which were 1/340 and 1/5 of the wild-type values, respectively. This mutational change caused a decrease of about 60-fold in enzymatic efficiency (k_{cat}/K_m). Replacing Glu526 with Gln and Ala

Table 1. Kinetic constants of AD2 wild-type and mutants for the hydrolysis of PNP-$(NAG)_2$. ND, not detected.

Enzyme	k_{cat} (s^{-1})	K_m (mM)	k_{cat}/K_m ($mM^{-1}\cdot s^{-1}$)
Wild-type	6.7 ± 0.4	0.46 ± 0.06	14.6 ± 2.1
D522N	2.36 ± 0.09	0.54 ± 0.07	4.3 ± 0.6
D522A	1.49 ± 0.04	0.74 ± 0.06	2.0 ± 0.2
D524N	2.47 ± 0.05	0.61 ± 0.04	4.1 ± 0.3
D524A	0.022 ± 0.001	0.09 ± 0.01	0.25 ± 0.04
E526Q	0.045 ± 0.002	0.12 ± 0.01	0.38 ± 0.04
E526A	ND		
W664A	0.022 ± 0.002	12.7 ± 2.1	0.0017 ± 0.0003

influenced the catalytic activity drastically. The E526Q mutation caused a reduction of about 130-fold in the wild-type k_{cat} value, and the E526A mutant abolished the enzymatic activity. Our kinetic results clearly demonstrate that Asp524 and Glu526 play important roles in the catalytic mechanism of AD2, whereas Asp522 has only a minor role.

Structural determination of AD2 mutants bound to chito-oligosaccharide substrate

The molecular activity (k_{cat}) of the AD2 E526A and D524A mutants was much lower than that of the wild-type (Table 1), and so we expected that these two mutants would be more suitable for observing the enzyme–substrate complex without any degradation of the substrate. We obtained crystals of these mutant enzymes complexed with chito-oligosaccharide substrate by means of cocrystallization and soaking methods, respectively, and determined their tertiary structures. We collected X-ray diffraction data for the AD2 E526A and D524A mutants and refined them to resolutions of 1.80 and 1.76 Å, respectively. A summary of crystallographic data collection and refinement statistics is given in Table 2.

Superimposition of the overall $(\beta/\alpha)_8$-barrel structures of AD2 wild-type (Protein Data Bank code 2DSK [23]), E526A and D524A mutants gave 300 equivalent C_α coordinates with r.m.s. deviations of approximately 0.3 Å (Fig. S1). Some small conformational differences were observed in the surface loop region comprising Gly488–Gly492 (a maximum C_α–C_α distance from the wild-type of 0.81 Å). However, these minor changes did not affect the overall structural integrity of these mutants compared with the wild-type (Fig. S1). Therefore, the significant depression of enzymatic activity by the introduction of E526A and D524A substitutions (Table 1) is not a result of conformational changes, but of the removal of negative charge at these residues.

Conformation of chito-oligosaccharides bound to the active site cleft

For the structural determination of the AD2–substrate complex, we used a NAG pentamer [$(NAG)_5$] as substrate. In the AD2 E526A mutant, on the surface of the active site cleft, a clear, connected electron density corresponding to $(NAG)_5$ was observed into which each NAG residue could fit. The NAG units in $(NAG)_5$ are numbered 1–5 from the nonreducing end towards the reducing end (i.e. NAG1–NAG5). We observed an electron density corresponding to $(NAG)_4$ in the AD2 D524A mutant. Presumably, this might be caused by a partial disorder of terminal NAG residues at the nonreducing end. We fitted the $(NAG)_4$ molecular model corresponding to NAG2–NAG5 of $(NAG)_5$

Table 2. Data collection and refinement statistics for AD2 E526A and D524A complexed with substrate.

Protein Data Bank code	3A4W	3A4X
Protein	E526A mutant	D524A mutant
Derivatization method[a]	Cocrystallization	Soaking
Diffraction data		
Space group	$P2_12_12_1$	$P2_12_12_1$
Unit cell parameters		
a (Å)	90.0	89.8
b (Å)	92.0	91.9
c (Å)	107.5	107.1
Number of observed reflections	596 577	641 671
Number of unique reflections	83 345	88 323
Resolution range (Å)[b]	30.0–1.80 (1.86–1.80)	50.0–1.76 (1.79–1.76)
Completeness (%)[b]	100 (100)	99.4 (90.4)
R_{merge} (%)[b,c]	9.0 (36.4)	9.1 (37.4)
I/σ (I)[b]	20.2 (5.7)	13.0 (2.2)
Redundancy[b]	7.2 (6.8)	7.3 (4.9)
B-factors of data from Wilson plot (Å^2)	10.5	11.3
Refinement		
Resolution range (Å)	29.5–1.80	37.8–1.76
R_{cryst}[d] (%)/R_{free}[e] (%)	15.4/17.4	15.3/17.5
R.m.s. deviations from ideality		
Bond length (Å)	0.011	0.011
Bond angle (deg)	1.30	1.43
Average of *B*-factor values		
All atoms (Å^2)	9.3	9.0
Main-chain (Å^2)	8.3	8.1
Side-chain (Å^2)	10.3	9.6
Substrate (Å^2)	8.5	12.5
Water (Å^2)	20.5	24.6
R.m.s. ΔB values		
Main-chain (Å^2)	0.6	0.6
Side-chain (Å^2)	2.0	1.8
Ramachandran plot statistics[f]		
Favored (%)	99.2	99.2
Allowed (%)	0.4	0.4
R.m.s. deviations of the two monomers in the asymmetric unit (Å)[g]	0.20	0.21

[a] See Experimental procedures. [b] Values in parentheses are for the highest resolution shells. [c] $R_{merge} = \Sigma|I - \langle I\rangle|/\Sigma I$, where I is the intensity of observation I and $\langle I\rangle$ is the mean intensity of the reflection. [d] $R_{cryst} = \Sigma||F_{obs}| - |F_{calc}||/\Sigma|F_{obs}|$, where F_{obs} and F_{calc} are the observed and calculated structure factor amplitudes, respectively. [e] R_{free} was calculated using a randomly selected 5% of the dataset that was omitted through all stages of refinement. [f] Ramachandran plots were created for all residues other than Gly and Pro. [g] R.m.s. deviations were calculated for 300 C_α atoms of the two molecules in the asymmetric unit.

in the E526A mutant into the electron density and carried out further refinements.

The final refined $2F_{obs} - F_{calc}$ maps of the substrates bound to AD2 E526A and D524A mutants are illustrated in Fig. 2. The conformations of $(NAG)_5$ in the E526A mutant and $(NAG)_4$ in the D524A mutant were almost identical, giving all matching atoms with an r.m.s. deviation of 0.10 Å, and they made a sharp turn at NAG3. Although NAG1, NAG2, NAG4 and NAG5 residues adopted standard $^4C_1$ chair conformations, the central NAG3 residue was distorted into the $^{1,4}B$ boat conformation. In addition, the dihedral angles of the third glycosidic bond (NAG3–NAG4) were very different from those of the other glycosidic bonds (NAG1–NAG2, NAG2–NAG3 and NAG4–NAG5) (Table 3). This similar distortion and twist of the bound substrate has been observed previously in the crystal structure of the bacterial chitinase ChiB from *Serratia marcescens* (SmChiB) complexed with $(NAG)_5$ [24,30]. AD2 causes the distortion and twisting of the substrate, so that the glycosidic oxygen faces towards the bottom of the deep cleft.

Enzyme–substrate interactions

The crystal structures of the AD2 E526A and D524A mutants complexed with substrate show that a number of amino acid residues contribute to the binding of the substrate by hydrogen bonding and/or hydrophobic interactions. Using the LIGPLOT program [31], we investigated the specific interactions between enzymes and each NAG residue in detail (Table 4). The most significant enzyme–substrate interactions were localized in NAG3, whose pyranose ring was distorted into the 'boat' conformation. Three residues (Ala490, Asp524 and Asp636) formed hydrogen bond interactions and six residues (Tyr421, Phe448, Met585, Met587, Met631 and Trp664) participated in hydrophobic interactions. We believe that these residues stabilize the distortion of the NAG3 residue. In these interactions, we particularly focused on the Trp664 residue, which is located at the bottom of the active site cleft. The indole ring of Trp664 is hydrophobically stacked with the pyranose ring of NAG3 (Fig. 2). We conducted kinetic analysis to discover the effect of the

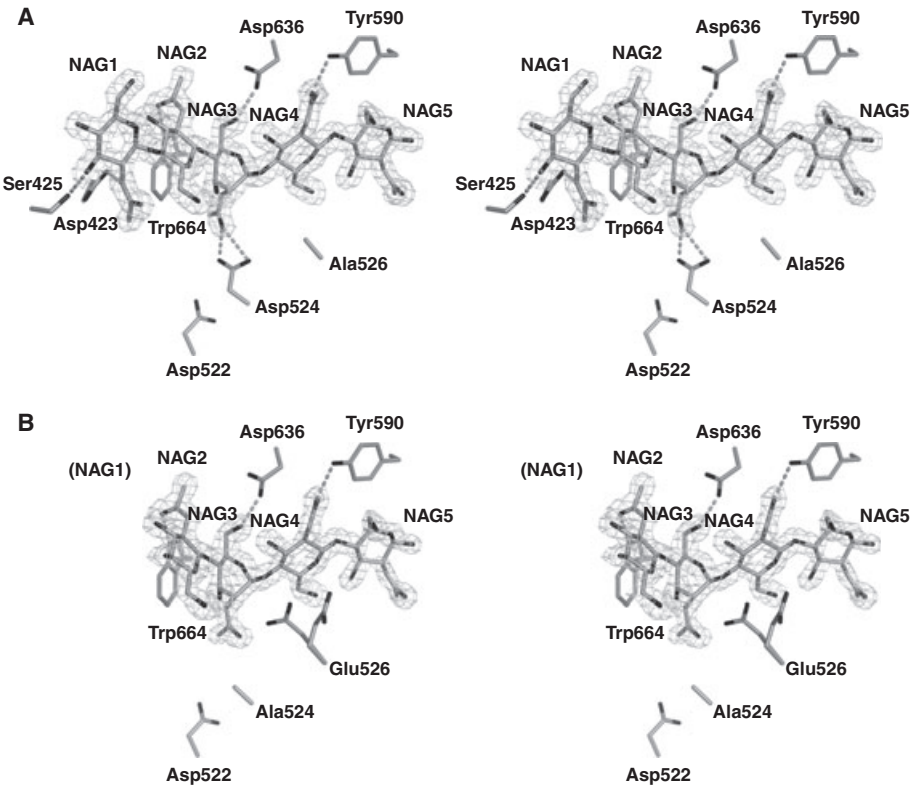

Fig. 2. Stereo figures of the model of the bound substrate in the AD2 E526A mutant (A) and D524A mutant (B). The structures of bound sugars and the side-chains of three acidic residues in the conserved DXDXE motif are indicated in a stick representation. The mesh represents $2F_{obs} - F_{calc}$ electron density maps contoured at the 1.5σ level. Residues involved in hydrogen bond interactions are also shown as sticks. The broken lines represent hydrogen bond interactions.

Table 3. Dihedral angles around the glycosidic bonds in the bound substrates. φ is the O5–C1–O4′–C4′ angle and ψ is the C1–O4′–C4′–C5′ angle, where O4 represents the oxygen of the glycosidic bond and atoms of the adjacent NAG unit are primed.

	E526A–substrate complex		D524A–substrate complex	
Glycosidic bond	φ	ψ	φ	ψ
NAG1–NAG2	−120.5	−162.5	–	–
NAG2–NAG3	−78.2	−151.0	−64.1	−150.8
NAG3–NAG4	−57.5	−98.0	−54.7	−87.3
NAG4–NAG5	−89.7	−161.4	−79.2	−163.7

W664A mutant (Table 1). This mutation decreased the wild-type k_{cat} value by 300-fold and increased the wild-type K_m value by 30-fold, reducing k_{cat}/K_m by about 9000-fold. We confirmed that hydrophobic stacking by Trp664 is crucial for both catalysis and substrate binding.

Characterization of acidic residues in the conserved DXDXE motif

Figure 3 shows a comparison of the crystal structures of the AD2 E526A–substrate and D524A–substrate complexes with that of the wild-type (substrate-free form) [23], focusing on the highly conserved DXDXE motif close to the bound substrate. The conformations of the bound substrate in E526A and D524A are almost identical, but the D524A mutation resulted in a remarkable change in the conformation of the Glu526 side-chain. The $2F_{obs} - F_{calc}$ electron density of the Glu526 side-chain in the D524A–substrate complex is not clear compared with that of the wild-type substrate-free form (Fig. 3A, C). However, the $F_{obs} - F_{calc}$ omit map of Glu526 clearly shows two conformers of this side-chain: the A- and B-form (Fig. 3C). We estimated the occupancy of the side-chain in these two conformers to be 0.5 : 0.5 using the CNS program [32]. In the wild-type substrate-free and D524A–substrate complex structures (Fig. 3A, C), the positions and orientations of the Glu526 side-chain in the A-form were almost identical, and the maximum coordinate shift after superimposition of the two structures was 0.78 Å. In the B-form, in contrast, the Glu526 side-chain rotated 55° around χ_1 relative to the A-form and was exposed to the solvent. The two oxygen atoms of the Glu526 side-chain in the A-form were positioned close to the proximal glycosidic oxygen atom (O1) at distances of 3.0 and 3.1 Å (Fig. 3C). This indicates that the hydrolytic reaction occurs at the third β-(1,4)-glycosidic bond between NAG3 and NAG4, and Glu526 acts as a catalytic proton donor. Therefore, AD2 possesses at least five sugar-binding subsites, −3, −2, −1, +1, +2, as shown in Fig. 3B.

Discussion

We performed mutational analyses of three conserved acidic residues (Asp522, Asp524 and Glu526) in AD2

Table 4. Hydrophobic and hydrogen bond interactions in the AD2 E526A and D524A mutants complexed with substrate.

	Hydrophobic interaction		Hydrogen bond interaction		
Sugar no.	Sugar atom	Protein residue	Sugar atom	Distance (Å)	Protein atom
NAG1 (−3)[a]	C7, C8	Ala461	N2	2.88	O_δ2 of Asp423
			O3	2.72	OH of Ser425
NAG2 (−2)	C6	Val491	O6	3.18	NH of Ala490
	C8	Val677	O7	2.84	NE1 of Trp664
	C8	Ser678			
NAG3 (−1)	C8	Tyr421	O3	2.89	NH of Ala490
	C7	Phe448	O6	2.64	O_δ2 of Asp636
	C1	Glu526[b]	O7	2.94	O_δ1 of Asp524[a]
	C7, C8	Met585	O7	2.40	O_δ2 of Asp524[a]
	C1	Met587			
	C6	Met631			
	C5, C6, C7, C8	Trp664			
NAG4 (+1)	C3	Ala490	O7	2.63	OH of Tyr590
	C4, C5, C6	Glu526[b]			
	C6	Met585			
NAG5 (+2)	C7,C8	Pro555			
	C8	Ser556			
	C5, C6	Tyr590			

[a] In the E526A–substrate complex only. [b] In the D524A–substrate complex only.

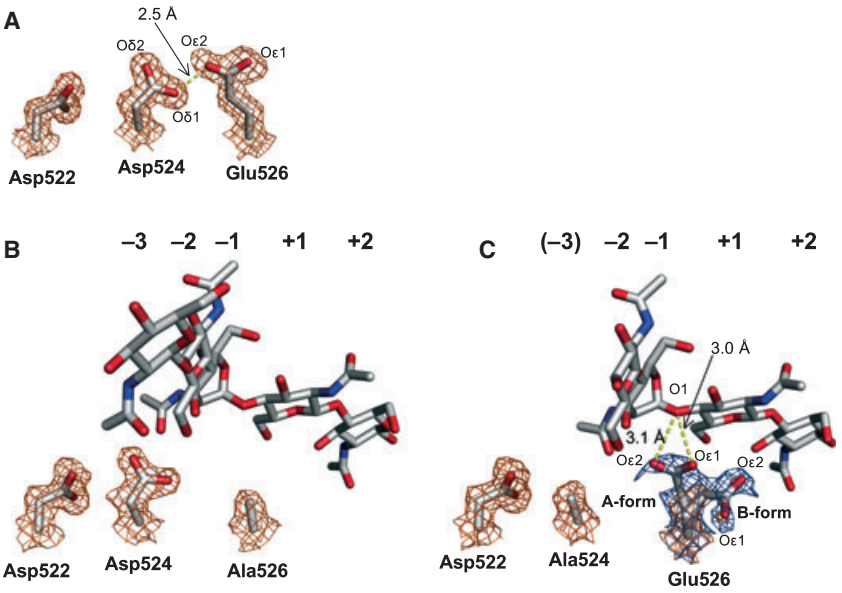

Fig. 3. Close-up views of the active site in the AD2 wild-type (A), E526A mutant (B) and D524A mutant (C). All structures are drawn from the same direction after superimposition. The side-chain structures are imposed onto a $2F_{obs} - F_{calc}$ electron density map (orange mesh), contoured at 1.2σ. In (C), the blue mesh represents an $F_{obs} - F_{calc}$ electron density map contoured at 2.4σ in which the Glu526 side-chain has been excluded from the calculation. The broken lines represent hydrogen bond interactions. Five subsites (–3, –2, –1, +1, +2) deduced from the solved structures are also shown, following the nomenclature system for sugar-binding subsites in GH [53].

and determined the structure of AD2 catalytic site mutants, E526A and D524A, complexed with $(NAG)_5$. To the best of our knowledge, these structures represent the first examples of an archaeal chitinase complexed with natural chito-oligosaccharide substrate.

So far, the three-dimensional structures of family 18 chitinases have been determined for hevamine from *Hevea brasiliensis* [19], chitinase 1 from *Saccharomyces cerevisiae* (ScCTS1) [33], chitinase B from *S. marcescens* (SmChiB) [22], chitinase 1 from *Coccidioides immitis* (CcCTS1) [21] and chitinase A1 from *Bacillus circulans* (BcChiA1) [20] (Fig. 4B–F). On the basis of their structures, family 18 chitinases are subclassified into 'plant-type' and 'bacterial-type' [33,34]. 'Plant-type' family 18 chitinases (hevamine and ScCTS1) contain a simple $(\beta/\alpha)_8$-barrel structure with a shallow substrate-binding groove (Fig. 4B, C), with one solvent-exposed tryptophan residue at the –1 subsite. As AD2 contains a simple $(\beta/\alpha)_8$-barrel fold with an open active site architecture, and has one tryptophan residue, Trp664, in the active site groove (Fig. 4A), archaeal chitinase AD2 belongs to the 'plant-type' family 18 chitinases. In contrast, 'bacterial-type' chitinases (SmChiB, CcCTS1 and BcChiA1) consist of the $(\beta/\alpha)_8$-barrel embellished with a tightly associated α/β-insertion domain and several long loops (Fig. 4D–F), resulting in a deep substrate-binding groove (cleft). This groove contains a large number of aromatic residues (Fig. 4D–F) which are thought to participate in substrate binding [35,36].

We used a combination of kinetic and crystallographic approaches to characterize the function of the DXDXE motif in AD2. Kinetic results showed that the carboxyl group of the Glu526 side-chain is essential for the enzymatic activity of AD2, and this group cannot be replaced by a neutral amide group (Table 1). In addition, the side-chain of Glu526 is located close to the scissile glycosidic bond (Fig. 3C). These results confirm that the acidic character of the carboxyl group of Glu526 has a catalytic proton-donating function as in other family 18 chitinases. The D524N mutant retained approximately 40% of the wild-type k_{cat} value, whereas the D524A mutant retained only 0.3% (Table 1). Thus, the carboxyl group of Asp524 is not necessarily indispensable and can be replaced by a neutral amide group for the catalytic activity, implying that the Asp524 side-chain participates in a hydrogen bond interaction with the bound substrate or proximal residues. Indeed, in the substrate-free wild-type structure, the Asp524 side-chain faces towards catalytic Glu526, forming a hydrogen bond between the O_ε atom of Glu526 and the O_δ atom of Asp524 in 2.5 Å (Fig. 3A). Interestingly, in the D524A–substrate complex, an altered conformation of the Glu526 side-chain (B-form) was observed in addition to the favorable conformer for proton transfer (A-form) (Fig. 3C). In the B-form, the shortest distance between the carboxyl oxygen atoms (O_ε) of the Glu526 side-chain and the scissile glycosidic oxygen atom (O1) is 5.0 Å. Accordingly, the B-form structure of the Glu526 side-chain is believed to be unable to donate a proton. In the substrate-free D524A mutant structure, on the other hand, only the A-form of catalytic Glu526 was observed (Table S1 and Fig. S2). The relative position of its side-chain was almost identical to that of the wild-type substrate-free form (Fig. 3A and Fig. S2B), despite the

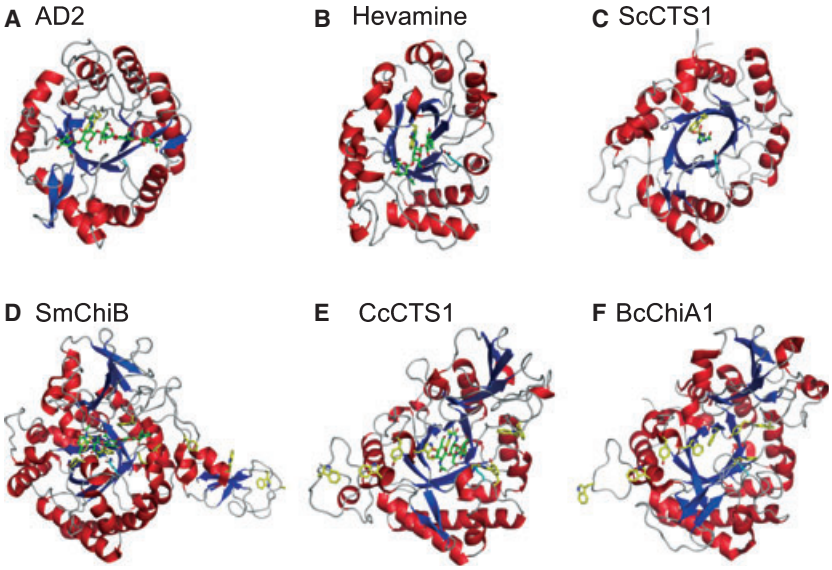

Fig. 4. Structural comparison of overall $(\beta/\alpha)_8$-folds for six family 18 chitinases. The overall structure of the AD2 E526A–substrate complex (A) is compared with the hevamine–allosamidin complex (Protein Data Bank code 1LLO) (B), ScCTS1–acetazolamide complex (Protein Data Bank code 2UY4) (C), SmChiB E144Q–$(NAG)_5$ complex (Protein Data Bank code 1E6N) (D), CcCTS1–allosamidin complex (Protein Data Bank code 1LL4) (E) and BcChiA1 substrate-free form (Protein Data Bank code 1ITX) (F). The β-strands and α-helices are denoted in blue and red, respectively. Catalytic Glu corresponding to Glu526 (replaced by Ala) in AD2 is shown as cyan carbon atoms. In the SmChiB–$(NAG)_5$ structure, catalytic Glu144 is replaced by Gln. Solvent-exposed aromatic residues lining the active site groove are shown as yellow carbon atoms. Substrate (inhibitor) structures are shown as green carbon atoms.

lack of hydrogen bond interaction between mutated Ala524 and Glu526. This suggests that the A-form is much more energetically favorable than the B-form, implying that an alternative B-form structure of catalytic Glu526 is induced by substrate binding onto the active site. From these results, taken together, we conclude that the Glu526 side-chain can adopt two conformers (A-form and B-form) in the substrate-bound form, and Asp524 acts to restrain the Glu526 side-chain into the A-form by hydrogen bond interaction, promoting Glu526 to donate a proton to a proximal glycosidic oxygen atom. The D524A–substrate complex is unique in that the substrate was detected in the active site of the D524A mutant, which does not completely lose catalytic activity (Table 1). It is possible that the conformational diversity of the Glu526 side-chain observed in this complex reflects movement during the catalytic cycle.

Through these structural analyses, we have found a remarkable difference between 'plant-type' and 'bacterial-type' family 18 chitinases in the conformational change of the second Asp (D_2) of the conserved DXDXE motif. Figure 5 focuses on the DXDXE motifs, comparing each structure in substrate-free and substrate-bound forms for 'plant-type' (AD2, hevamine, ScCTS1; Fig. 5A–C) and 'bacterial-type' (SmChiB, CcCTS1, BcChiA1; Fig. 5D–F) chitinases. For BcChiA1, only the substrate-free form structure is displayed because no substrate-bound structure is available (Fig. 5F). The crystallographic studies of SmChiB and CcCTS1 have demonstrated that catalysis by these 'bacterial-type' chitinases involves a conformational change of the second Asp (D_2) in the DXDXE motif on substrate binding (Fig. 5D, E) [24,37]. Thus, the D_2 residue interacts with catalytic Glu (E) and the first Asp (D_1) in the presence and absence of the bound substrate, respectively (Fig. 5D, E). This 'flip'-like conformational change may also play an important role in 'cycling' the pK_a of catalytic Glu during catalysis [24,38]. The mutation of the D_1 residue to Asn (D140N) in SmChiB caused a 500-fold decrease in activity [39]. On the other hand, in 'plant-type' chitinases (AD2, hevamine and ScCTS1), the side-chain of the D_2 residue always faces towards the catalytic Glu whether the substrate binds or not (Fig. 5A–C), and so does not interact directly with the adjacent D_1 residue. For AD2, the shortest distance between the side-chain atoms of Asp522 (D_1) and Asp524 (D_2) is actually 4.4 Å in the wild-type substrate-free structure (Fig. 3A). Kinetic results showed that the D522A mutant retained approximately 20% of its wild-type k_{cat} value. These crystallographic and kinetic results clearly demonstrate that, for 'plant-type' chitinase, the carboxyl group of the side-chain of the

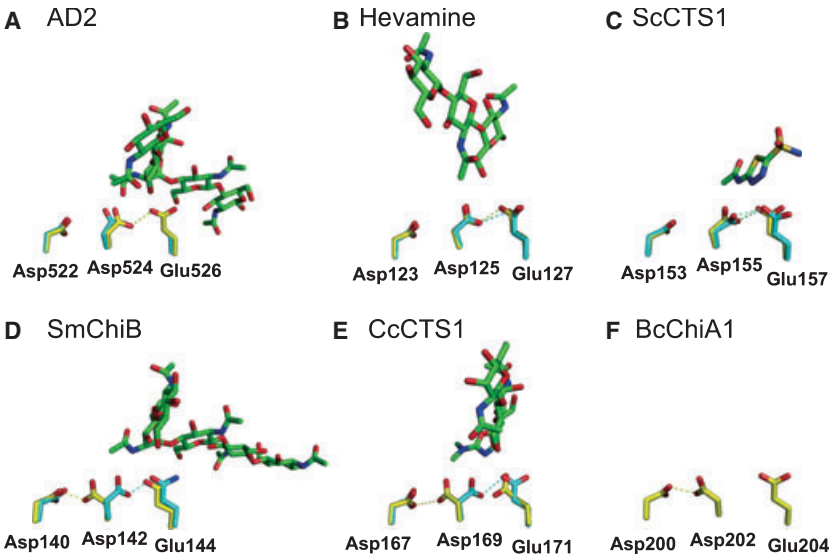

Fig. 5. Structural comparison of active sites for six family 18 chitinases, focusing on the conserved DXDXE motif. The close-up view of the active site in AD2 (A) is compared with hevamine (Protein Data Bank code 2HVM and 1LLO) (B), ScCTS1 (Protein Data Bank code 2UY2 and 2UY4) (C), SmChiB (Protein Data Bank code 1E15 and 1E6N) (D), CcCTS1 (Protein Data Bank code 1D2K and 1LL4) (E) and BcChiA1 (Protein Data Bank code 1ITX) (F). Each diagram is the superimposition of ligand (substrate or inhibitor)-free and ligand-bound structures. In (F), only the ligand-free structure is shown because no ligand-bound structure is available. The side-chains of three DXDXE acidic residues in ligand-free and ligand-bound forms are shown as yellow and cyan carbon atoms, respectively. Ligand structures are shown as green carbon atoms. Hydrogen bond interactions are indicated by broken lines, which are the same color as protein side-chain structures.

D_1 residue in the DXDXE motif is not involved directly in the catalytic mechanism, but participates in the hydrogen bond network which stabilizes the core of the $(\beta/\alpha)_8$-barrel. Thus, we may propose a new criterion for the classification of 'plant-type' and 'bacterial-type' family 18 chitinases based on the conformational change of the second Asp residue in the DXDXE motif on substrate binding.

As suggested by X-ray crystallographic analyses of SmChiB, catalysis in family 18 chitinases involves the *N*-acetyl group of the sugar bound at the –1 subsite of the enzyme (substrate-assisted catalysis) [24,40–42]. Protonation of the glycosidic bond by catalytic Glu leads to a distortion of the sugar residue at the −1 subsite into a 'boat' conformation, and the departure of the group is accompanied by a nucleophilic attack by the *N*-acetyl oxygen (O7) on the anomeric carbon (C1), thus yielding a positively charged, transient, oxazolinium ion intermediate. In the AD2 E526A–substrate structure, the *N*-acetyl oxygen of the −1 sugar faces towards Asp524, which is opposite to the direction in which it points in the SmChiB–$(NAG)_5$ structure (Fig. 6) [24]. The *N*-acetyl oxygen (O7) is located far from the anomeric carbon (C1) in an unfavorable position for a direct nucleophilic attack on the C1 carbon by the O7 oxygen (Fig. 6A). Therefore, a drastic flip-like conformational change of the

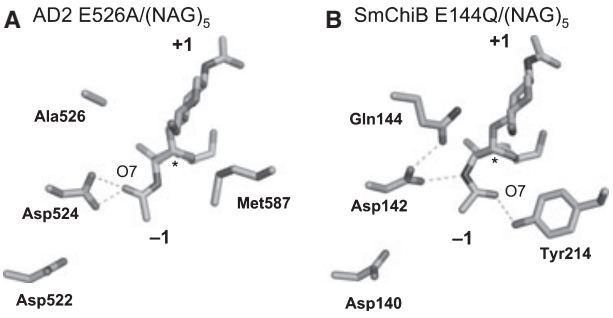

Fig. 6. Comparison of the active sites in the AD2 E526A–$(NAG)_5$ (A) and SmChiB E144Q–$(NAG)_5$ (B) complexes (Protein Data Bank code 1E6N), focusing on the conformation of bound substrates. For clarity, only the sugar residues at subsites –1 and +1 are shown. In the structures of AD2 and SmChiB, catalytic Glu (Glu526 and Glu144) is replaced by Ala and Gln, respectively. The Tyr residue, which is highly conserved among family 18 chitinases, is replaced by Met in AD2. The anomeric carbons (C1), which are subjected to nucleophilic attack by the carbonyl oxygen (O7) of the *N*-acetyl group, are represented by asterisks. Hydrogen bond interactions are shown as broken lines.

N-acetyl group should occur during the catalytic cycle of AD2. In the current proposed catalytic models, conserved Tyr residues (Tyr214 in SmChiB, Tyr183 in hevamine) cooperate with the DXDXE motif to help the catalytic reactions by stabilizing substrate distortion (Fig. 6B) [22,24,40]. In AD2, however, this residue

is replaced by Met, which does not seem to interact with *N*-acetyl groups by forming a hydrogen bond in a similar manner to Tyr (Fig. 6A) [23]. In the catalytic mechanism of AD2, an oxazolinium ion intermediate could be formed with the assistance of an amino acid residue other than the DXDXE motif, as originally proposed by Tews *et al.* [43] This is simpler than the mechanism of the other family 18 chitinases.

Experimental procedures

Site-directed mutagenesis and enzyme purification

Site-directed mutagenesis was introduced into a plasmid vector pET32_AD2$_{Pf\text{-}ChiA}$ [29] with the 'QuikChange Site-directed Mutagenesis Kit' (Stratagene, La Jolla, CA, USA) according to the manufacturer's protocol, with a minor modification: instead of *Pfu* DNA polymerase, we used KOD plus polymerase (TOYOBO, Osaka, Japan). Target primers for the generation of D522N, D522A, D524N, D524A, E526Q, E526A and W664A mutations were 5′-GCCACT TACTTG**AAC**TTTGACATAGAAGCCGG-3′, 5′-GCCAC TTACTTG**GCA**TTTGACATAGAAGCC-3′, 5′-GCCACT TACTTGGACTTT**AAC**ATAGAAGCCGG-3′, 5′-GCCAC TTACTTGGACTTT**GCG**ATAGAAGCCGG-3′, 5′-GGAC TTTGACATA**CAA**GCCGGTATCGATGC-3′, 5′-GGACT TTGACATA**GCG**GCCGGTATCGATGC-3′ and 5′-GGA TCACTAGCCTTC**GCG**AGTGTAGACAGAG-3′, respectively, in which the mutated codons are in bold. The resulting recombinant plasmids were verified by DNA sequencing with an ABI Prism® 310 Genetic Analyzer (Applied Biosystems, Foster City, CA, USA) and transformed into expression host *E. coli* Rosetta (DE3) cells.

Overexpression and purification of all recombinant AD2 mutants were carried out using the same procedure as described for the wild-type enzyme [29]. Briefly, cultures were produced in Luria–Bertani (LB) broth containing 50 μg·mL^{-1} of ampicillin at 37 °C; enzyme expression was induced with 0.5 mM isopropyl-1-thio-β-D-galactopyranoside and purification was conducted by a combination of immobilized metal affinity chromatography using a HiTrap Chelating HP column (GE Healthcare, Little Chalfont, Buckinghamshire, UK) and anion-exchange chromatography using a HiTrap Q HP column (GE Healthcare). Enzyme purity was assessed by SDS/PAGE [44], followed by Coomassie brilliant blue staining. The enzyme concentration was determined using UV absorbance at 280 nm and calculated extinction coefficients [29].

Enzymology

The kinetic constants k_{cat} and K_m of the AD2 wild-type and mutants were determined using the chromogenic substrate PNP-$(NAG)_2$ (Seikagaku Co., Tokyo, Japan) [45]. Standard reaction mixtures contained purified enzyme and 0.01–5 mM of PNP-$(NAG)_2$ in 0.2 M sodium acetate buffer (pH 4.8) to a final volume of 400 μL. Enzyme concentrations were adapted to the varying activities of the AD2 mutants. Reaction mixtures were incubated for 10 min at 50 °C, after which the reaction was terminated with the addition of 400 μL of 2 M sodium carbonate buffer (pH 10.1). The amount of released *p*-nitrophenol was quantified spectrophotometrically by the absorbance at 405 nm. The standard employed *p*-nitrophenol at a concentration range covering those of the substrates used in the kinetic experiments. The production of *p*-nitrophenol was linear with time for the incubation period, and < 5% of the available substrate was hydrolyzed. The initial velocity was saturable with increasing substrate concentration, and the best-fit values of the apparent kinetic constants, k_{cat} and K_m, in the Michaelis-Menten equation were obtained using nonlinear regression analysis with ORIGIN software (OriginLab Co., Northampton, MA, USA).

Crystallization

We used AD2 E526A and D524A mutants to determine the AD2–substrate complex structure. An E526A mutant complexed with chito-oligosaccharides was cocrystallized by the hanging drop vapor diffusion method. A portion (1 μL) of E526A enzyme solution [20 mg·mL^{-1} in 20 mM Tris/HCl (pH 8.0), 50 mM NaCl] was mixed with 1 μL of reservoir solution [0.1 M Mes (pH 6.5), 1.6 M $MgSO_4$] containing 5 mM $(NAG)_5$ (chitopentaose; Seikagaku Co., Tokyo, Japan), and equilibrated against 0.35 mL of reservoir solution at 25 °C. Crystals suitable for X-ray diffraction measurement appeared within 1 week in the drops at a maximum size of 0.1 mm × 0.1 mm × 0.5 mm. We obtained crystals of the D524A mutant complexed with chito-oligosaccharides by soaking experiments. Substrate-free D524A crystals were prepared using procedures similar to those employed previously for the wild-type [29]. A single D524A crystal was soaked for 30 min at room temperature in a reservoir solution [0.1 M Mes (pH 6.5), 1.6 M $MgSO_4$] containing 5 mM $(NAG)_5$.

X-Ray crystal structure determination

X-Ray diffraction data were collected using 0.90 Å synchrotron radiation at the undulator beamline BL44XU at SPring-8 (Harima, Japan). For data collection, the crystals were cryoprotected in the reservoir solution [0.1 M Mes (pH 6.5), 1.6 M $MgSO_4$] supplemented with 20% glycerol (v/v), followed by flash cooling at 100 K by a nitrogen gas stream. Diffraction data were integrated and scaled using the programs DENZO and SCALEPACK from the HKL2000 package [46]. Cross-validation was applied by excluding 5% of the reflections throughout the refinement procedure (free

R-factor) [47]. All refinements were initiated by rigid body refinement with REFMAC in the CCP4 suite [48,49], followed by substrate model building. Substrate starting structures and topologies were generated with the PRODRG server [50]. The molecular models were built using COOT [51] based on $2F_{obs} - F_{calc}$ and $F_{obs} - F_{calc}$ electron density maps, and were improved through many steps by alternate cycles of manual model modification and crystallographic restrained refinement with REFMAC until the *R*-factor and free *R*-factor converged. Occupancy refinement for two conformers of the Glu526 side-chain observed in the D524A–substrate complex (Fig. 3C, see Results for details) was carried out using the CNS program [32]. The stereochemistry of the model (structural validation) was analyzed using PROCHECK [52]. The data collection and refinement statistics are summarized in Table 2. For the final model, the structures of the two independent monomers in the asymmetric unit were almost identical (Table 2). In the interest of simplicity, the structures are discussed consistently using the first monomer of the coordinate files, unless otherwise stated. The structures and electron density maps were created and displayed using the PYMOL program (http://www.pymol.org).

Acknowledgements

The authors thank Ms C. Kageyama for technical assistance with protein purification and crystallization and Dr Joseph Rodrigue for critical reading of the manuscript. The X-ray diffraction studies were carried out at the Japan Synchrotron Radiation Research Institute.

References

1 Cottrell MT, Moore JA & Kirchman DL (1999) Chitinases from uncultured marine microorganisms. *Appl Environ Microbiol* **65**, 2553–2557.
2 Bhattacharya D, Nagpure A & Gupta RK (2007) Bacterial chitinases: properties and potential. *Crit Rev Biotechnol* **27**, 21–28.
3 Keyhani NO & Roseman S (1999) Physiological aspects of chitin catabolism in marine bacteria. *Biochim Biophys Acta* **1473**, 108–122.
4 Kuranda MJ & Robbins PW (1991) Chitinase is required for cell separation during growth of *Saccharomyces cerevisiae*. *J Biol Chem* **266**, 19758–19767.
5 Sahai AS & Manocha MS (1993) Chitinases of fungi and plants: their involvement in morphogenesis and host–parasite interaction. *FEMS Microbiol Rev* **11**, 317–338.
6 Leah R, Tommerup H, Svendsen I & Mundy J (1991) Biochemical and molecular characterization of three barley seed proteins with antifungal properties. *J Biol Chem* **266**, 1564–1573.
7 Collinge DB, Kragh KM, Mikkelsen JD, Nielsen KK, Rasmussen U & Vad K (1993) Plant chitinases. *Plant J* **3**, 31–40.
8 Melchers LS, Apotheker-de Groot M, van der Knaap JA, Ponstein AS, Sela-Buurlage MB, Bol JF, Cornelissen BJ, van den Elzen PJ & Linthorst HJ (1994) A new class of tobacco chitinases homologous to bacterial exo-chitinases displays antifungal activity. *Plant J* **5**, 469–480.
9 Jeuniaux C (1961) Chitinase: an addition to the list of hydrolases in the digestive tract of vertebrates. *Nature* **192**, 135–136.
10 Zhu Z, Zheng T, Homer RJ, Kim YK, Chen NY, Cohn L, Hamid Q & Elias JA (2004) Acidic mammalian chitinase in asthmatic Th2 inflammation and IL-13 pathway activation. *Science* **304**, 1678–1682.
11 Donnelly LE & Barnes PJ (2004) Acidic mammalian chitinase: a potential target for asthma therapy. *Trends Pharmacol Sci* **25**, 509–511.
12 Kawada M, Hachiya Y, Arihiro A & Mizoguchi E (2007) Role of mammalian chitinases in inflammatory conditions. *Keio J Med* **56**, 21–27.
13 Henrissat B (1991) A classification of glycosyl hydrolases based on amino acid sequence similarities. *Biochem J* **280**, 309–316.
14 Henrissat B & Bairoch A (1993) New families in the classification of glycosyl hydrolases based on amino acid sequence similarities. *Biochem J* **293**, 781–788.
15 Henrissat B & Davies G (1997) Structural and sequence-based classification of glycoside hydrolases. *Curr Opin Struct Biol* **7**, 637–644.
16 Hart PJ, Pfluger HD, Monzingo AF, Hollis T & Robertus JD (1995) The refined crystal structure of an endochitinase from *Hordeum vulgare* L. seeds at 1.8 Å resolution. *J Mol Biol* **248**, 402–413.
17 Hoell IA, Dalhus B, Heggset EB, Aspmo SI & Eijsink VG (2006) Crystal structure and enzymatic properties of a bacterial family 19 chitinase reveal differences from plant enzymes. *FEBS J* **273**, 4889–4900.
18 Perrakis A, Tews I, Dauter Z, Oppenheim AB, Chet I, Wilson KS & Vorgias CE (1994) Crystal structure of a bacterial chitinase at 2.3 Å resolution. *Structure* **2**, 1169–1180.
19 Terwisschavan Scheltinga AC, Hennig M & Dijkstra BW (1996) The 1.8 Å resolution structure of hevamine, a plant chitinase/lysozyme, and analysis of the conserved sequence and structure motifs of glycosyl hydrolase family 18. *J Mol Biol* **262**, 243–257.
20 Matsumoto T, Nonaka T, Hashimoto M, Watanabe T & Mitsui Y (1999) Three-dimensional structure of the catalytic domain of chitinase A1 from *Bacillus circulans* WL-12 at a very high resolution. *Proc Jpn Acad Ser B* **75**, 269–274.
21 Hollis T, Monzingo AF, Bortone K, Ernst S, Cox R & Robertus JD (2000) The X-ray structure of a chitinase

from the pathogenic fungus *Coccidioides immitis*. *Protein Sci* **9**, 544–551.
22 van Aalten DM, Synstad B, Brurberg MB, Hough E, Riise BW, Eijsink VG & Wierenga RK (2000) Structure of a two-domain chitotriosidase from *Serratia marcescens* at 1.9-Å resolution. *Proc Natl Acad Sci USA* **97**, 5842–5847.
23 Nakamura T, Mine S, Hagihara Y, Ishikawa K & Uegaki K (2007) Structure of the catalytic domain of the hyperthermophilic chitinase from *Pyrococcus furiosus*. *Acta Crystallogr Sect F: Struct Biol Cryst Commun* **63**, 7–11.
24 van Aalten DM, Komander D, Synstad B, Gåseidnes S, Peter MG & Eijsink VG (2001) Structural insights into the catalytic mechanism of a family 18 exo-chitinase. *Proc Natl Acad Sci USA* **98**, 8979–8984.
25 Oku T & Ishikawa K (2006) Analysis of the hyperthermophilic chitinase from *Pyrococcus furiosus*: activity toward crystalline chitin. *Biosci Biotechnol Biochem* **70**, 1696–1701.
26 Tanaka T, Fujiwara S, Nishikori S, Fukui T, Takagi M & Imanaka T (1999) A unique chitinase with dual active sites and triple substrate binding sites from the hyperthermophilic archaeon *Pyrococcus kodakaraensis* KOD1. *Appl Environ Microbiol* **65**, 5338–5344.
27 Dahiya N, Tewari R & Hoondal GS (2006) Biotechnological aspects of chitinolytic enzymes: a review. *Appl Microbiol Biotechnol* **71**, 773–782.
28 Nakamura T, Mine S, Hagihara Y, Ishikawa K, Ikegami T & Uegaki K (2008) Tertiary structure and carbohydrate recognition by the chitin-binding domain of a hyperthermophilic chitinase from *Pyrococcus furiosus*. *J Mol Biol* **381**, 670–680.
29 Mine S, Nakamura T, Hirata K, Ishikawa K, Hagihara Y & Uegaki K (2006) Crystallization and X-ray diffraction analysis of a catalytic domain of hyperthermophilic chitinase from *Pyrococcus furiosus*. *Acta Crystallogr Sect F: Struct Biol Cryst Commun* **62**, 791–793.
30 Papanikolau Y, Prag G, Tavlas G, Vorgias CE, Oppenheim AB & Petratos K (2001) High resolution structural analyses of mutant chitinase A complexes with substrates provide new insight into the mechanism of catalysis. *Biochemistry* **40**, 11338–11343.
31 Wallace AC, Laskowski RA & Thornton JM (1995) LIGPLOT: a program to generate schematic diagrams of protein–ligand interactions. *Protein Eng* **8**, 127–134.
32 Brünger AT, Adams PD, Clore GM, DeLano WL, Gros P, Grosse-Kunstleve RW, Jiang JS, Kuszewski J, Nilges M, Pannu NS *et al.* (1998) Crystallography & NMR system: a new software suite for macromolecular structure determination. *Acta Crystallogr D: Biol Crystallogr* **54**, 905–921.
33 Hurtado-Guerrero R & van Aalten DM (2007) Structure of *Saccharomyces cerevisiae* chitinase 1 and screening-based discovery of potent inhibitors. *Chem Biol* **14**, 589–599.
34 Rao FV, Houston DR, Boot RG, Aerts JM, Hodkinson M, Adams DJ, Shiomi K, Omura S & van Aalten DM (2005) Specificity and affinity of natural product cyclopentapeptide inhibitors against *A. fumigatus*, human, and bacterial chitinases. *Chem Biol* **12**, 65–76.
35 Watanabe T, Ariga Y, Sato U, Toratani T, Hashimoto M, Nikaidou N, Kezuka Y, Nonaka T & Sugiyama J (2003) Aromatic residues within the substrate-binding cleft of *Bacillus circulans* chitinase A1 are essential for hydrolysis of crystalline chitin. *Biochem J* **376**, 237–244.
36 Katouno F, Taguchi M, Sakurai K, Uchiyama T, Nikaidou N, Nonaka T, Sugiyama J & Watanabe T (2004) Importance of exposed aromatic residues in chitinase B from *Serratia marcescens* 2170 for crystalline chitin hydrolysis. *J Biochem* **136**, 163–168.
37 Bortone K, Monzingo AF, Ernst S & Robertus JD (2002) The structure of an allosamidin complex with the *Coccidioides immitis* chitinase defines a role for a second acid residue in substrate-assisted mechanism. *J Mol Biol* **320**, 293–302.
38 Kolstad G, Synstad B, Eijsink VG & van Aalten DM (2002) Structure of the D140N mutant of chitinase B from *Serratia marcescens* at 1.45 Å resolution. *Acta Crystallogr D: Biol Crystallogr* **58**, 377–379.
39 Synstad B, Gåseidnes S, Vriend G, Nielsen JE & Eijsink VGH (2000) On the contribution of conserved acidic residues to the catalytic activity of chitinase B from *Serratia marcescens*. In *Advances in Chitin Science*, Vol. 4 (Peter MG, Muzzarelli RAA & Domard A, eds), pp. 524–529. European Chitin Society.
40 Bokma E, Rozeboom HJ, Sibbald M, Dijkstra BW & Beintema JJ (2002) Expression and characterization of active site mutants of hevamine, a chitinase from the rubber tree *Hevea brasiliensis*. *Eur J Biochem* **269**, 893–901.
41 Synstad B, Gåseidnes S, van Aalten DM, Vriend G, Nielsen JE & Eijsink VG (2004) Mutational and computational analysis of the role of conserved residues in the active site of a family 18 chitinase. *Eur J Biochem* **271**, 253–262.
42 Vaaje-Kolstad G, Houston DR, Rao FV, Peter MG, Synstad B, van Aalten DM & Eijsink VG (2004) Structure of the D142N mutant of the family 18 chitinase ChiB from *Serratia marcescens* and its complex with allosamidin. *Biochim Biophys Acta* **1696**, 103–111.
43 Tews I, Terwisscha van Scheltinga AC, Perrakis A, Wilson KS & Dijkstra BW (1997) Substrate-assisted catalysis unifies two families of chitinolytic enzymes. *J Am Chem Soc* **119**, 7954–7959.
44 Laemmli UK (1970) Cleavage of structural proteins during the assembly of the head of bacteriophage T4. *Nature* **227**, 680–685.

45 Suginta W, Songsiriritthigul C, Kobdaj A, Opassiri R & Svasti J (2007) Mutations of Trp275 and Trp397 altered the binding selectivity of *Vibrio carchariae* chitinase A. *Biochim Biophys Acta* **1770**, 1151–1160.
46 Otwinowski Z & Minor W (1997) Processing of X-ray diffraction data collected in oscillation mode. *Methods Enzymol* **276**, 307–326.
47 Brünger AT (1992) Free *R* value: a novel statistical quantity for assessing the accuracy of crystal structures. *Nature* **355**, 472–475.
48 Collaborative Computational Project, Number 4 (1994) The CCP4 suite: programs for protein crystallography. *Acta Crystallogr D: Biol Crystallogr* **50**, 760–763.
49 Murshudov GN, Vagin AA & Dodson EJ (1997) Refinement of macromolecular structures by the maximum-likelihood method. *Acta Crystallogr D: Biol Crystallogr* **53**, 240–255.
50 Schüttelkopf AW & van Aalten DM (2004) PRODRG: a tool for high-throughput crystallography of protein–ligand complexes. *Acta Crystallogr D: Biol Crystallogr* **60**, 1355–1363.
51 Emsley P & Cowtan K (2004) Coot: model-building tools for molecular graphics. *Acta Crystallogr D: Biol Crystallogr* **60**, 2126–2132.
52 Laskowski RA, Moss DS & Thornton JM (1993) Main-chain bond lengths and bond angles in protein structures. *J Mol Biol* **231**, 1049–1067.
53 Davies GJ, Wilson KS & Henrissat B (1997) Nomenclature for sugar-binding subsites in glycosyl hydrolases. *Biochem J* **321**, 557–559.

Supporting information

The following supplementary material is available:
Fig. S1. Overall structures of AD2 catalytic site mutants complexed with chito-oligosaccharides.
Fig. S2. Structure of AD2 D524A substrate-free form.
Table S1. Data collection and refinement statistics for the AD2 D524A substrate-free form.

This supplementary material can be found in the online version of this article.

Please note: As a service to our authors and readers, this journal provides supporting information supplied by the authors. Such materials are peer-reviewed and may be re-organized for online delivery, but are not copy-edited or typeset. Technical support issues arising from supporting information (other than missing files) should be addressed to the authors.